Journal of Chromatography, 517 (1990) 521–547
Elsevier Science Publishers B.V., Amsterdam

CHROMSYMP. 1938

Influence of thermal variation of diffusion coefficient on non-equilibrium plate height in capillary zone electrophoresis

JOE M. DAVIS
Department of Chemistry and Biochemistry, Southern Illinois University at Carbondale, Carbondale, IL 62901 (U.S.A.)

ABSTRACT

A numerical algorithm is developed by which the radial profiles of temperature and mobility in an electrophoretic capillary can be computed from the steady-state equation of heat conduction. To determine these profiles accurately, the viscosity at any temperature is calculated to four significant figures from an expression different from the commonly used Andrade equation. The profiles so computed are used in a theory derived here, which addresses the impact of the thermal variation of diffusion coefficient on the axial dispersion of analyte ions in capillary zone electrophoresis. The magnitude of this dispersion is expressed as the non-equilibrium plate height. The numerical computation of this plate height indicates that this variation becomes significant only when the difference in temperature between the capillary center and wall exceeds *ca.* 5°C. The plate heights computed here can differ by more than a factor of two from those based on the Andrade equation, even when the variation of the diffusion coefficient is ignored. These differences originate from the relative inaccuracy of this equation.

INTRODUCTION

This paper addresses the influence of the thermal variation of diffusion coefficient on the non-equilibrium plate height of analyte ions in capillary zone electrophoresis (CZE). The origin of non-equilibrium dispersion in CZE is the gradient in temperature caused by the Joule heating of the capillary contents. Because electrophoretic mobilities increase with temperature, analyte ions migrate faster near the capillary center, where the temperature is higher, than near the capillary wall, where the temperature is lower. The resultant dispersion is mitigated by the radial diffusion of analyte ions, which averages out these differences in velocity to some degree.

Other theories for the non-equilibrium plate height or the effective diffusion coefficient, which is proportional to this plate height, in CZE have been derived. (As shown below, the effective diffusion coefficient is a calculated measure of the axial dispersion caused by the radial variation of analyte velocity.) Many of these theories

0021-9673/90/$03.50

differ only slightly from one another. By representing the Poiseuille flow in an open tube by three discrete components, Konstantinov and Oshurkova[1] derived an approximate effective diffusion coefficient analogous to that of Taylor[2,3]. Martin and Everaerts[4] suggested an analogy between the effective diffusion coefficient for chromatography, as derived by Golay[5], and that for CZE. Cox *et al.*[6] approximated the radial variation of analyte velocity by an equation derived by Hjertén[7]; he then solved the equation of continuity, from which the plate height was calculated, by making an analogy with the work of Aris[8]. In a work closely related to that of Konstantinov and Oshurkova[1], Virtanen[9] calculated an effective diffusion coefficient for CZE by modifying Taylor's effective diffusion coefficient for dispersion in open tubes. Similarly, Knox and Grant[10] modified Taylor's theory of dispersion to calculate the non-equilibrium plate height. Most recently, Grushka *et al.*[11] adapted the theory of Reejhsinghani *et al.*[12] to calculate from the equation of continuity an effective diffusion coefficient, from which the non-equilibrium plate height was evaluated.

A common attribute among these theories is the calculation (by a variety of means) of the mean square axial displacement of the analyte from the mean analyte position. The random-walk theory of dispersion shows that this result is proportional to the time required for ions to diffuse between two characteristic positions in the capillary, at which their velocities significantly differ[13]. In all of the above theories, this time is approximated as a constant. Because the diffusion coefficient of analyte ions increases with temperature, however, the time required for ions to diffuse from one position to another is reduced near the capillary center, where the temperature is higher, relative to that near the capillary wall, where the temperature is lower. In other words, this time is not constant but varies with the radial position in the capillary. No attempt has been made to determine under what conditions this approximation breaks down and the radial variation of the diffusion coefficient becomes important. This paper does so.

In some of the theories referenced above, detailed equations for plate height were evaluated with analytical expressions for the temperature and electrophoretic mobility of analyte ions in the capillary. In general, these expressions apply when the difference in temperature between the capillary wall and center is vanishingly small. They are only approximately correct, however, when this temperature difference is large, *i.e.*, when non-equilibrium dispersion is large. Because the temperature difference, above which the variation of diffusion coefficient is important, is unknown (indeed, its determination is the goal of the paper), one does not know *a priori* if these expressions are appropriate for this study. To obtain a fairly rigorous solution, these expressions are not used here except in limiting cases. Instead, expressions for the temperature and electrophoretic mobility are computed numerically from the steady-state equation of heat conduction. These expressions are free of all but the most fundamental assumptions and are, in principle, applicable over a wide range of temperatures.

THEORY

The theory of this paper is composed of two parts. In Part I, the profiles of temperature and electrophoretic mobility are computed from the steady-state equation of heat conduction. In Part II, an expression for the non-equilibrium plate height is derived, in which the radial variation of the diffusion coefficient is addressed.

Numerical values of this expression are then evaluated with the temperature and mobility profiles computed in Part I.

Part I: Determination of radial temperature and electrophoretic-mobility profiles

Here, one will assume that thermal convection, thermal diffusion, and heat transfer from electroosmotically induced forced convection are negligible. One will also assume the analyte concentration is vanishingly small, such that the electrical and thermal properties of the capillary contents are determined by the buffer only, and the analyte does not alter the electric field strength. Finally, one will assume that the equilibrium constants governing the dissociation of the buffer and analyte do not vary over the range of temperatures experienced by the buffer. (These assumptions will be critiqued later.) The radial temperature profile in the capillary is then governed by the steady-state equation of heat conduction[14,15]

$$-\frac{1}{r}\frac{\mathrm{d}}{\mathrm{d}r}\left[rk_t(r)\frac{\mathrm{d}T(r)}{\mathrm{d}r}\right] = k_e(r)E^2 \tag{1}$$

where r is the radial coordinate, $T(r)$ is temperature, $k_t(r)$ and $k_e(r)$ are the thermal and electrical conductivities of the buffer, and E is the electric field strength. Although one should strictly interpret the conductivities $k_e(r)$ and $k_t(r)$ as functions of radial coordinate r[14,15], one alternatively can (as commonly does) interpret them as functions of temperature $T(r)$ (ref. 15). By introducing the variables

$$y = \frac{r}{a};\ \theta(y) = \frac{T(y) - T_o}{T_o} \tag{2}$$

one can reexpress eqn. 1 in the dimensionless form[14]

$$-\frac{1}{y}\frac{\mathrm{d}}{\mathrm{d}y}\left[y\frac{k_t(y)}{k_{to}}\frac{\mathrm{d}\theta(y)}{\mathrm{d}y}\right] = \frac{k_e(y)}{k_{eo}}B \tag{3}$$

where a is the capillary radius, T_o is the temperature at the (inner) capillary wall, k_{to} and k_{eo} are the thermal and electrical conductivities of the buffer at this wall, and B is

$$B = \frac{k_{eo}a^2E^2}{k_{to}T_o} \tag{4}$$

Several solutions to eqn. 3 have been developed, which differ in the approximations chosen for the reduced conductivities $k_e(y)/k_{eo}$ and $k_t(y)/k_{to}$. When these approximations equal the constant, one (*i.e.*, when the conductivities are independent of temperature); the solution to eqn. 3 is simply

$$\lim_{B\to 0}\theta(y) = \frac{B}{4}(1 - y^2) \tag{5}$$

Others have solved eqn. 3 more rigorously to address the dependences of $k_e(y)/k_{eo}$ and

$k_t(y)/k_{to}$ on temperature. Broer[14] expressed these functions as two-term expansions in $\theta(y)$ and so accounted for the linear variations with temperature of the electrical and thermal conductivities. By equating $k_t(y)/k_{to}$ to one and $k_e(y)/k_{eo}$ to a two-term expansion in $\theta(y)$, Coxon and Binder[16], Brown and Hinckley[17], and Jones and Grushka[18] obtained Bessel functions as solutions to eqn. 3. These functions account for only the linear variation with temperature of the electrical conductivity.

The most general solution to eqn. 3, subject to the boundary conditions $d\theta(y)/dy = 0|_{y=0}$ (because of radial symmetry) and $\theta(y) = 0|_{y=1}$ (because $T = T_o$ at the wall), is

$$\theta(y) = B\int_0^1 \frac{1}{\left[\frac{k_t(y)}{k_{to}}\right]_y}\left[\int_0^y \frac{k_e(y)}{k_{eo}} y\,dy\right]dy = B\int_0^1 \frac{1}{h(y)y}\left[\int_0^y f(y)y\,dy\right]dy \tag{6a}$$

$$f(y) = k_e(y)/k_{eo};\ h(y) = k_t(y)/k_{to} \tag{6b}$$

where the ratios, $k_e(y)/k_{eo}$ and $k_t(y)/k_{to}$, are now represented by the functions $f(y)$ and $h(y)$, respectively. These functions vary with the radial coordinate y because the conductivities vary with temperature. In other words, $h(y)$ and $f(y)$ vary with $T(y) = T_o[1 + \theta(y)]$. But $\theta(y)$ is unknown; it is the function one seeks. In solving eqn. 6a, one is saddled with the circular task of determining $\theta(y)$ from two functions which themselves depend on $\theta(y)$.

A general solution to eqn. 6a is developed here, but not because the solutions to $\theta(y)$ referenced above are inadequate. Rather, as will be shown below, the non-equilibrium plate height depends on the function $f(y)$, which describes the radial variation of the electrophoretic mobility. By judiciously developing the solution to eqn. 6a, one can determine $f(y)$ without any assumptions beyond those outlined at the beginning of this section. To achieve this objective, one must sacrifice analytical rigor for numerical methods. As compensation, however, one circumvents the shortcomings that others have encountered in the derivation of approximations to $f(y)$, especially for large values of B.

An iterative numerical algorithm by which $f(y)$ can be computed is now outlined. For any value of B, one can solve eqn. 6a numerically by initially equating $f(y)$ and $h(y)$ to one. In this case, the solution to $\theta(y)$ is eqn. 5, within numerical error. For any value of T_o, this solution to $\theta(y)$ defines the temperature T at all values of y (in this case, $T = T_o[1 + B(1 - y^2)/4]$, from which new approximations to $f(y)$ and $h(y)$ can then be calculated from empirical functions of temperature for the electrical and thermal conductivities. In other words, the temperature at any coordinate y defines the values of the electrical and thermal conductivities at that coordinate; the ratios of that electrical conductivity to k_{eo}, and that thermal conductivity to k_{to}, define the values of the functions $f(y)$ and $h(y)$, respectively, at that coordinate. One can then substitute these new approximations to $f(y)$ and $h(y)$ into eqn. 6a, numerically integrate with respect to y, and compute a new solution to $\theta(y)$. This solution will differ from the previous one, because the functions $f(y)$ and $h(y)$ now differ from one. From this new solution to $\theta(y)$, one can again calculate the temperature at all values of y and new approximations to $f(y)$ and $h(y)$, as before. One can iteratively repeat this algorithm,

until f(y), h(y), and $\theta(y)$ converge to constant values. When this convergence is reached, then one has an excellent approximation to the function f(y) that one needs to describe the radial variation of electrophoretic mobility.

To implement this algorithm, one must have accurate functions for h(y) and f(y) at different temperatures. These functions will be represented by $h[T(y)] = h[T_o, \theta(y)]$ and $f[T(y)] = f[T_o,\theta(y)]$, respectively. Over the temperature range, 7–97°C, the function $h[T_o,\theta(y)]$ for water can be described with an accuracy of one part per thousand [at least, for the values 280, 290, 300, ..., 370 K (ref. 19)] by the quadratic

$$h[T_o,\theta(y)] = 1 + \alpha_1\theta(y) + \alpha_2\theta(y)^2 \tag{7}$$

where

$$\alpha_1 = (6.090 \cdot 10^{-3} T_o - 1.511 \cdot 10^{-5} T_o^2)/\Delta \tag{7a}$$

$$\alpha_2 = -7.555 \cdot 10^{-6} T_o^2/\Delta \tag{7b}$$

$$\Delta = -0.5390 + 6.090 \cdot 10^{-3} T_o - 7.555 \cdot 10^{-6} T_o^2 \tag{7c}$$

and where T_o is expressed in degrees Kelvin. These equations were determined by fitting a quadratic function of T to tabulated values of the thermal conductivity of water[19] and then by reexpressing $T = T(y)$ in terms of $\theta(y)$, eqn. 2. The function Δ (eqn. 7c) is the quadratic approximation to the thermal conductivity of water at the temperature T_o, in W/(mK). Lest any ambiguity exist in the use of eqn. 7, one should perhaps again state that the value of $h[T_o,\theta(y)]$ at coordinate y in a given iteration is determined from T_o and the value of $\theta(y)$ computed at that coordinate in the previous iteration. Eqn. 7, although determined for water, is also adequate for electrolytic buffers, because salts contribute to the thermal conductivity by an amount less than $2 \cdot 10^{-5}$ W/(mK) or so per ion, as long as their molar concentration is less than 0.1 (ref. 20), a concentration which is rarely exceeded in CZE.

The function $f[T_o,\theta(y)]$ is developed from the electrical conductivity $k_e(T)$, which is[21]

$$k_e(T) = F\sum_i z_i(T)|\mu_i(T)|C_i(T) = eF\sum_i \frac{z_i^2(T)}{f_{ri}(T)}C_i(T) \tag{8}$$

where F is the Faraday constant; e is the fundamental electrical charge; and z_i μ_i, C_i, and f_{ri} are the unsigned number of charges, the electrophoretic mobility, the concentration, and the friction coefficient of the ith ion, respectively. If one neglects the variation of z_i and C_i with temperature (the former, from changes in screening by the electrical double layer, extent of ionization, etc.; the latter, from volume expansion), then eqn. 8 may be expressed as

$$k_e(T) = \frac{eF}{\eta(T)}\sum \frac{A_i^*}{A_i(T)} \tag{9}$$

where A_i^* equals the constant $z_i^2 C_i$ and the explicit dependence of friction coefficient f_r on viscosity η has been expressed as $f_{ri}(T) = A_i(T)\eta(T)$. If one now assumes that the plane of hydrodynamic shear (and hence the effective ionic radius) is independent of temperature, then A_i is also independent of temperature. Consequently, as first shown by Hjertén[7], $f[T_o,\theta(y)]$ can be approximated as

$$f[T_o, \theta(y)] = \frac{\eta_o}{\eta[T_o, \theta(y)]} \tag{10}$$

where η_o is the viscosity at the inner capillary wall.

Many empirical equations have been proposed to describe the dependence of viscosity on temperature[20]. Here, two such functions for the viscosity η of water are critiqued. Over the temperature range, 15–100°C, η can be described to four significant figures by[22]

$$\eta = \eta_{293} 10^{\frac{1.3272(293-T) - 1.053\cdot 10^{-3}(293-T)^2}{T-168}} \tag{11}$$

where T is expressed in degrees Kelvin and η_{293} is the viscosity of water at 293 K. This empirical equation accurately predicts to four significant figures values of viscosity measured to five significant figures[23]. By combining eqns. 10 and 11, one can express $f[T_o,\theta(y)]$ as

$$f[T_o,\theta(y)] = 10^{T_o[\beta_1\theta(y) + \beta_2\theta(y)^2]/\beta_3} \tag{12a}$$

where

$$\beta_1 = 165.9 + (1.053 \cdot 10^{-3})(293 - T_o)(43 - T_o) \tag{12b}$$

$$\beta_2 = (1.053 \cdot 10^{-3})T_o(T_o - 168) \tag{12c}$$

$$\beta_3 = (T_o - 168)\{T_o[\theta(y) + 1] - 168\} \tag{12d}$$

For small values of B, eqn. 12 can be linearized by expanding eqn. 12a as a two-term Taylor series, neglecting the quadratic power of $\theta(y)$ in this expansion, and neglecting $\theta(y)$ in coefficient β_3. The result is

$$\lim_{B\to 0} f(y) \approx 1 + \alpha\theta(y) = 1 + \alpha B\frac{(1 - y^2)}{4} \tag{13a}$$

$$\alpha = \frac{\ln(10)\beta_1 T_o}{(T_o - 168)^2} \tag{13b}$$

where $\theta(y)$ has been approximated by eqn. 5.

In other studies[7,11], η alternatively was represented by the Andrade equation[20]

$$\eta = \eta^* e^{B_A/T} \tag{14}$$

for which

$$f[T_o, \theta(y)] = e^{B_A\theta(y)/\{T_o[1+\theta(y)]\}} \tag{15}$$

where B_A is an empirical temperature commonly equated to 2400 K. By representing this equation by a two-term Taylor-series expansion and expressing $\theta(y)$ in this expansion by eqn. 5, others showed[7,11]

$$\lim_{B\to 0} f(y) \approx 1 + \frac{B_A}{T_o} B \frac{(1-y^2)}{4} \tag{16}$$

The expansions, eqns. 13 and 16, are clearly different; they are equal only when T_o satisfies the equation

$$B_A = \frac{\ln(10)\beta_1 T_o^2}{(T_o - 168)^2} \tag{17}$$

or when $T_o \approx 4°C(B_A = 2400$ K). At all other temperatures, eqns. 13 and 16 will predict different values for the variation of electrophoretic mobility with temperature and consequently the non-equilibrium plate height.

In spite of its common use, eqn. 14 describes the variation of η with temperature somewhat poorly. In support of this assertion, Table I reports estimates of η calculated from eqns. 11 and 14 for selected temperatures grouped in intervals of two degrees. This two-degree interval was chosen as an arbitrary upper limit to the temperature difference between the capillary center and wall that one might encounter in CZE, under experimental conditions where Joule heating is marginal. For each group, the parameter η^* was computed by fitting to eqn. 14 ($B_A = 2400$ K) with least-squares methods the three values of η computed from eqn. 11. The η values so calculated agree with those calculated from eqn. 11 only to within two significant figures. Also, the variation of η^* from group to group is substantial, which indicates that a larger temperature range could not be spanned by eqn. 14 with any accuracy. These equations predict different values of η at different temperatures, principally because they have different values of $d\eta/dT$.

The differences between these values raise some doubts about the accuracy of electrophoretic mobilities calculated from the Andrade equation. In this paper, eqn. 11 will be used for this task, unless otherwise stated. As will be shown below, these differences are so substantial that eqn. 16 predicts non-equilibrium plate heights that can be 150% larger than those predicted by eqn. 13, other factors being equal.

Part II: Derivation of non-equilibrium plate height for radially dependent diffusion coefficient

Here, the dispersion theory of Reejhsinghani *et al.*[12] is used to address the influence of the radial variation of the analyte diffusion coefficient on the non-equilibrium plate height in CZE. This theory draws heavily on Taylor's studies of dispersion[2,3] and was also used by Grushka *et al.*[11] in a recent calculation of plate height, in which this variation was ignored. In essence, this theory simplifies the

TABLE I

COMPARISON OF VISCOSITIES η CALCULATED FROM EQNS. 11 AND 14

Parameter η^* was determined by least-squares regression.

T (°C)	*Eqn. 11*	*Eqn. 14*	$\eta^* \cdot 10^4$ *(cP)*
25	0.8905	0.8942	
26	0.8705	0.8704	2.843
27	0.8513	0.8475	
35	0.7194	0.7231	
36	0.7053	0.7051	2.986
37	0.6916	0.6877	
45	0.5960	0.5995	
46	0.5856	0.5855	3.163
47	0.5755	0.5719	
55	0.5041	0.5074	
56	0.4962	0.4962	3.369
57	0.4885	0.4854	
65	0.4335	0.4365	
66	0.4274	0.4275	3.600
67	0.4214	0.4187	
75	0.3781	0.3805	
76	0.3732	0.3731	3.848
77	0.3685	0.3658	
85	0.3337	0.3359	
86	0.3298	0.3297	4.119
87	0.3259	0.3236	

equation of continuity to an ordinary differential equation, whose solution determines an effective diffusion coefficient from which the plate height is calculated. The theory developed below may be construed as an extension of these more fundamental works.

One develops this ordinary differential equation from the equation of continuity in radial coordinates, which is[14]

$$\frac{\partial c}{\partial t} + \frac{1}{r}\frac{\partial}{\partial r}(rN_r) + \frac{\partial N_z}{\partial z} = 0 \tag{18}$$

where N_r and N_z are respectively the one-dimensional radial and axial fluxes

$$N_r = v_r c - D_r \frac{\partial c}{\partial r} \tag{19}$$

$$N_z = v_z c - D_z \frac{\partial c}{\partial z} \tag{20}$$

and where z is the axial coordinate, t is time, $c = c(r,z,t)$ is the analyte concentration, and v_r and v_z (D_r and D_z) are the analyte velocities (diffusion coefficients) in the radial and axial directions. No angular flux appears, because of radial symmetry. If one again assumes that thermal convection and thermal diffusion are negligible, then $v_z = v_z(r)$ is

$$v_z(r) = [\mu(r) + \mu_{eo}]E \tag{21}$$

where $\mu(r)$ is the electrophoretic mobility at coordinate r and μ_{eo} is the electroosmotic flow coefficient (both μ and μ_{eo} are signed quantities). Here, one has assumed that capillary diameters are sufficiently large that one can neglect the variation of electroosmotic flow in the electrical double layer at the capillary–buffer interface. Hence, the electroosmotic flow equals $\mu_{eo}E$. One has also assumed that the steady-state equation of heat conduction applies and that v_z does not vary with t, as it does during a brief initial transient[16].

The mobility can be expressed as $\mu(r) = -\varepsilon\zeta/\eta(r)$ (ref. 24), where ε and ζ are the electrical permittivity of the buffer and the zeta potential of the analyte. If one neglects the variation of these parameters with temperature, eqn. 21 may be expressed as[7,11]

$$v_z(r) = \left\{-\frac{\varepsilon\zeta}{\eta_o}\left[\frac{\varepsilon\zeta/\eta(r)}{\varepsilon\zeta/\eta_o}\right] + \mu_{eo}\right\}E = [\mu_o f(r) + \mu_{eo}]E \tag{22}$$

where $\mu_o = -\varepsilon\zeta/\eta_o$ is the electrophoretic mobility of the analyte at the capillary wall and $f(r)$ is the equivalent of $f(y)$, but now expressed in terms of the dimensioned coordinate, r, instead of the dimensionless coordinate, $y = r/a$. (For the moment, equations in r are more convenient than equations in y; the final results will be expressed in terms of y.) Eqn. 22 marks the first appearance of the function $f(r)$ [or $f(y)$], which is determined numerically as described in Part I.

If one now assumes that D_z is independent of z and that thermal diffusion is negligible (*i.e.*, that $v_r = 0$), then the substitution of eqns. 19 and 20 into eqn. 18 yields

$$\frac{\partial c}{\partial t} + v_z(r)\frac{\partial c}{\partial z} = \frac{1}{r}\frac{\partial}{\partial r}\left[rD_r(r)\frac{\partial c}{\partial r}\right] + D_z\frac{\partial^2 c}{\partial z^2} \tag{23}$$

where the dependence of $D_r = D_r(r)$ on radial coordinate r is expressed explicitly.

By defining the coordinate $z_1 = z - \bar{v}t$, where $\bar{v}$ is the average analyte velocity in the axial direction, one can implement the standard coordinate transformation

$$\left(\frac{\partial c}{\partial t}\right)_z = \left(\frac{\partial c}{\partial t}\right)_{z_1} - \bar{v}\left(\frac{\partial c}{\partial z_1}\right)_t \tag{24}$$

with which eqn. 23 can be expressed as

$$\frac{\partial c}{\partial t} + [v_z(r) - \bar{v}]\frac{\partial c}{\partial z_1} = \frac{1}{r}\frac{\partial}{\partial r}\left[rD_r(r)\frac{\partial c}{\partial r}\right] + D_z\frac{\partial^2 c}{\partial z_1^2} \tag{25}$$

The theory of Reejhsinghani *et al.*[12] is now used to simplify eqn. 25. First, the concentration c is approximated by the two-term expansion

$$c = c_m(z_1) + \frac{\partial c_m(z_1)}{\partial z_1} g(r) \tag{26}$$

where $c_m(z_1)$ is the cross sectional average concentration (2)

$$c_m(z_1) = \frac{2}{a^2}\int_0^a rc\,dr \tag{27}$$

and $g(r)$ is a function to be determined. By combining eqns. 26 and 27, one can show[12]

$$\int_0^a rg(r)dr = 0 \tag{28}$$

which will prove useful later.

Because $c_m(z_1)$ is independent of r, and derivatives of $c_m(z_1)$ with respect to z_1 of order two or greater are negligible compared to $\partial c_m(z_1)/\partial z_1$ (ref. 12), the following additional approximations hold

$$\frac{\partial c}{\partial r} \approx \frac{\partial c_m(z_1)}{\partial z_1}\frac{dg(r)}{dr} \tag{29a}$$

$$\frac{\partial^2 c}{\partial r^2} \approx \frac{\partial c_m(z_1)}{\partial z_1}\frac{d^2 g(r)}{dr^2} \tag{29b}$$

$$\frac{\partial c}{\partial z_1} \approx \frac{\partial c_m(z_1)}{\partial z_1} \tag{29c}$$

$$\frac{\partial c}{\partial t} \approx 0 \tag{29d}$$

By substituting eqn. 29 into eqn. 25 and neglecting derivatives of $c_m(z_1)$ with respect to z_1 of order two or greater, one obtains the ordinary differential equation

$$v_z(r) - \bar{v} = \frac{1}{r}\frac{d}{dr}\left[rD_r(r)\frac{dg(r)}{dr}\right] \tag{30}$$

which integrates to

$$\int_0^r r[v_z(r) - \bar{v}]dr = rD_r(r)\frac{dg(r)}{dr} \tag{31}$$

where the right-hand side, $rD_r(r)\mathrm{d}g(r)/\mathrm{d}r$, equals zero at $r = 0$ (the lower limit of the integral on the left-hand side), because $\mathrm{d}g(r)/\mathrm{d}r$ equals zero at $r = 0$. (Obviously, the right-hand side is also zero at $r = 0$, because the first factor of this function is r.) The function $\mathrm{d}g(r)/\mathrm{d}r$ equals zero at $r = 0$, because the diffusive flux

$$-D_r(r)\frac{\partial c}{\partial r} = -D_r(r)\frac{\partial c_m(z_1)}{\partial z_1}\frac{\mathrm{d}g(r)}{\mathrm{d}r} \tag{32}$$

is zero at $r = 0$, because of radial symmetry. Because neither $D_r(r)$ nor $\partial c_m(z_1)/\partial z_1$ is zero at $r = 0$, eqn. 32 equals zero at $r = 0$ only if $\mathrm{d}g(r)/\mathrm{d}r$ equals zero at $r = 0$. This function is also zero at $r = a$, because analyte cannot diffuse across the capillary wall. This latter equality will prove most useful later.

If the radial gradient in temperature is the only cause of the radial variation of $D_r(r)$, one can express this variation as[20,25]

$$\frac{D_r(r)\eta(r)}{T(r)} = A' \tag{33}$$

where A' is a constant, whose value depends on the physical properties of the analyte and buffer. The theoretical origin of this expression is the Nernst–Haskell equation, which describes the mutual diffusion coefficient of a salt at infinite dilution[20,25]. Eqn. 33 is also theoretically justified for molecular species by the Stokes–Einstein equation[20,25], which in turn forms the basis of the empirical equations for the mutual diffusion coefficient of Wilke and Chang[20,25]; Tyn and Calus[20]; Nakanishi[20]; King, Hsueh and Mao[25]; and Reddy and Doraiswamy[25].

With eqn. 33, one can express the ratio of $D_r(r)$ to D_{ro}, the value of $D_r(r)$ at the capillary wall, as

$$\frac{D_r(r)}{D_{ro}} = \frac{A'T(r)/\eta(r)}{A'T_o/\eta_o} = \mathrm{f}(r)\frac{T(r)}{T_o} = \mathrm{f}(r)[\theta(r) + 1] \tag{34}$$

from which one concludes

$$D_r(r) = D_{ro}\mathrm{f}(r)[\theta(r) + 1] \tag{35}$$

where $\theta(r)$ is the equivalent of $\theta(y)$, but expressed in terms of r, instead of y.

By substituting eqn. 35 for $D_r(r)$ in eqn. 31, one can show

$$\mathrm{g}(r) - \mathrm{g}(0) = \frac{1}{D_{ro}}\int_0^r \frac{1}{r\mathrm{f}(r)[\theta(r) + 1]}\int_0^r r[v_z(r) - \bar{v}]\mathrm{d}r\mathrm{d}r \tag{36}$$

where $\mathrm{g}(0)$ is the value of $\mathrm{g}(r)$ at $r = 0$. Eqn. 36 alternatively can be expressed in terms of coordinate $y = r/a$ as

$$\mathrm{g}(y) - \mathrm{g}(0) = \frac{a^2\mu_o E}{D_{ro}}\int_0^y \frac{1}{y\mathrm{f}(y)[\theta(y) + 1]}\int_0^y y\left[\mathrm{f}(y) - 2\int_0^1 y\mathrm{f}(y)\mathrm{d}y\right]\mathrm{d}y\mathrm{d}y \tag{37}$$

where $v_z(r)$ is expressed by eqn. 22 and the average zone velocity $\bar{v}$ is

$$\bar{v} = 2\int_0^1 y v_z(y)\mathrm{d}y = [2\mu_o(\int_0^1 y f(y)\mathrm{d}y + \mu_{eo}]E \tag{38}$$

in accordance with this equation. One observes that μ_{eo} subtracts out in this result; the electroosmotic flow causes no dispersion.

A brief outline of the calculation of the non-equilibrium plate height from eqn. 37 may be appropriate here, because Reejhsinghani *et al.*[12] provide little detail in their work, and Grushka *et al.*[11] simply cite their result (actually, its negative). The analysis below differs from that of Reejhsinghani *et al.*[12] as best as the author can tell, but it parallels that of Giddings in his plate-height studies of chromatography[13] and field-flow fractionation[26]. In any case, the result is the same as that derived by Reejhsinghani *et al.* The average convective flux, $<cv_z(r)>$, in the axial direction can be expressed with eqn. 26 as

$$<cv_z(r)> = \frac{2c_m(z_1)}{a^2}\int_0^a r v_z(r)\mathrm{d}r + \frac{2}{a^2}\frac{\partial c_m(z_1)}{\partial z_1}\int_0^a r g(r) v_z(r)\mathrm{d}r \tag{39}$$

The first term in this equation equals the average convective flux, $c_m(z_1)\bar{v}$, which represents the translation of the average zone concentration at the average zone velocity. The second term represents a dispersive flux, which alternatively can be expressed by Fick's first law, $-\mathscr{D}\partial c_m(z_1)/\partial z_1$, where $\mathscr{D}$ is an effective diffusion coefficient equal to

$$\mathscr{D} = -\frac{2}{a^2}\int_0^a r g(r) v_z(r)\mathrm{d}r \tag{40a}$$

$$= -2\int_0^1 y g(y) v_z(y)\mathrm{d}y \tag{40b}$$

and from which the non-equilibrium plate height H is calculated as $2\mathscr{D}/\bar{v}$ (refs. 11, 13 and 26)

$$H = -\frac{4}{a^2\bar{v}}\int_0^a r g(r) v_z(r)\mathrm{d}r = -\frac{4}{\bar{v}}\int_0^1 y g(y) v_z(y)\mathrm{d}y \tag{41}$$

So far, the theory developed here parallels that of Grushka *et al.*[11], except that the radial variation of diffusion coefficient has been included. Now, a slight departure is taken. One does not need to determine the constant of integration g(0) in eqn. 37, as did Grushka *et al.*[11], to evaluate eqn. 41, because this latter equation also equals

$$H = -\frac{4}{\bar{v}}\int_0^1 y[g(y) - g(0)][v_z(y) - \bar{v}]\mathrm{d}y \tag{42a}$$

$$= -\frac{4\mu_o E}{\bar{v}}\int_0^1 y[g(y) - g(0)]\left[f(y) - 2\int_0^1 yf(y)dy\right]dy \tag{42b}$$

To demonstrate this equality, one expands eqn. 42a to the result

$$H = -\frac{4}{\bar{v}}\left[\int_0^1 yg(y)v_z(y)dy - \bar{v}\int_0^1 yg(y)dy - g(0)\int_0^1 yv_z(y)dy + g(0)\bar{v}\int_0^1 ydy\right] \tag{43}$$

The second term in this expansion equals zero, by virtue of eqn. 28. The third and fourth terms respectively equal $-g(0)\bar{v}/2$ and $+g(0)\bar{v}/2$ and cancel one another, regardless of the value of g(0). (In fact, they cancel one another, regardless of the lower limit of the outermost integral in eqn. 37. Advantages accrue if one chooses $y = 0$ as the lower limit, however, as will be shown below.) Only the first term, which equals eqn. 41, remains. This simplification of theory is identical to that developed by Giddings[26] in his non-equilibrium theory of field-flow fractionation.

By combining eqns. 37 and 42b, one can express H as

$$H = -\frac{4(a\mu_o E)^2}{D_{ro}\bar{v}}\int_0^1 y\left[f(y) - 2\int_0^1 yf(y)dy\right]\int_0^y \frac{1}{yf(y)[\theta(y) + 1]}\int_0^y y\left[f(y) - 2\int_0^1 yf(y)dy\right]dydydy \tag{44}$$

This cumbersome result fortunately can be simplified substantially by integration by parts, in a manner identical to that developed by Giddings[27] in the non-equilibrium theory of field-flow fractionation. If one lets

$$U = \int_0^y \frac{1}{yf(y)[\theta(y) + 1]}\int_0^y y\left[f(y) - 2\int_0^1 yf(y)dy\right]dydy \tag{45}$$

and

$$dV = y\left[f(y) - 2\int_0^1 yf(y)dy\right]dy \tag{46}$$

then eqn. 44 can be expressed as

$$H = -\frac{4(a\mu_o E)^2}{D_{ro}\bar{v}}\int_0^1 UdV = -\frac{4(a\mu_o E)^2}{D_{ro}\bar{v}}\left[UV\Big|_0^1 - \int_0^1 VdU\right] \tag{47}$$

where $UV\Big|_0^1$ implies that $U(y = 1)$ and $V(y = 1)$, and $U(y = 0)$ and $V(y = 0)$, are multiplied, and that the latter product is subtracted from the former. The function

$$V = \int y\left[\mathrm{f}(y) - 2\int_0^1 y\mathrm{f}(y)\mathrm{d}y\right]\mathrm{d}y \tag{48}$$

is the dimensionless equivalent of eqn. 31, which is zero at both $r = 0$ and $r = a$ ($y = 0$ and $y = 1$), because $\mathrm{d}g(r)/\mathrm{d}r$ equals zero at both these limits (see discussion immediately following eqn. 31). Therefore, the first term, $UV\Big|_0^1$, equals zero, and eqn. 47 reduces to

$$H = \frac{4(a\mu_o E)^2}{D_{ro}\bar{v}}\int_0^1 V\mathrm{d}U = \frac{4(a\mu_o E)^2}{D_{ro}\bar{v}}\int_0^1 \frac{1}{y\mathrm{f}(y)[\theta(y)+1]}\left\{\int_0^y y\left[\mathrm{f}(y) - 2\int_0^1 y\mathrm{f}(y)\mathrm{d}y\right]\mathrm{d}y\right\}^2\mathrm{d}y \tag{49}$$

where one has now taken advantage of the equality, $V(y = 0) = 0$, to express the product of two integrals as the square of the same integral.

Eqn. 49 can be expressed in the dimensionless form

$$\frac{HD_{ro}\bar{v}}{(a\mu_o E)^2} = 4\int_0^1 \frac{1}{y\mathrm{f}(y)[\theta(y)+1]}\left\{\int_0^y y\left[\mathrm{f}(y) - 2\int_0^1 y\mathrm{f}(y)\mathrm{d}y\right]\mathrm{d}y\right\}^2\mathrm{d}y \tag{50}$$

which is the desired theoretical result.

In general, eqn. 50 must be evaluated numerically, because $\mathrm{f}(y)$ and $\theta(y)$ are computed numerically, as detailed in Part I. For small values of B, however, an analytical solution can be determined by approximating $\theta(y)$ and $\mathrm{f}(y)$ in eqn. 50 by eqns. 5 and 13, respectively. In this case, eqn. 50 integrates to the somewhat awkward result

$$\lim_{B\to 0}\frac{HD_{ro}\bar{v}}{(a\mu_o E)^2} = \frac{\alpha}{16} + \frac{2\alpha^2}{B^2(1-\alpha)}\left[\left(1+\frac{B}{4}\right)\ln\left(1+\frac{B}{4}\right) - \frac{B}{4}\right] - \frac{2}{B^2\alpha(1-\alpha)}\left[\left(1+\frac{\alpha B}{4}\right)\ln\left(1+\frac{\alpha B}{4}\right) - \frac{\alpha B}{4}\right] \tag{51}$$

where α is defined by eqn. 13b. By using the expansion

$$\left(1+\frac{\gamma}{4}\right)\ln\left(1+\frac{\gamma}{4}\right) - \frac{\gamma}{4} \approx \frac{\gamma^2}{32} - \frac{\gamma^3}{384} + \frac{\gamma^4}{3072} - \frac{\gamma^5}{20480} + \cdots \tag{52}$$

where γ is any real number, one can approximate eqn. 51 by

$$\lim_{B\to 0}\frac{HD_{ro}\bar{v}}{(a\mu_o E)^2} \approx \frac{1}{1536}\left[\frac{\ln(10)\beta_1 T_o B}{(T_o - 168)^2}\right]^2\left\{1 - \frac{3B}{20}\left[1 + \frac{\ln(10)\beta_1 T_o}{(T_o - 168)^2}\right]\right\} \tag{53}$$

where T_o is in degrees Kelvin, α has been explicitly expressed, and β_1 is defined by eqn. 12b.

To test this theory, one should compare eqn. 50 to the analytical result derived by Grushka *et al.*[11]. To make this comparison, one must "turn off" the radial variation of the diffusion coefficient in eqn. 50 by equating the functions f(y) and $\theta(y)$ to one and zero, respectively, in the expression, $\{yf(y)[\theta(y) + 1]\}^{-1}$. In this case, eqn. 50 becomes

$$\lim_{D_r(r)\to D_{ro}} \frac{HD_{ro}\bar{v}}{(a\mu_o E)^2} = 4\int_0^1 \left\{\frac{1}{y}\int_0^y \left[y\left[f(y) - 2\int_0^1 yf(y)dy\right]dy\right]\right\}^2 dy \tag{54}$$

If f(y) in eqn. 54 is now equated to eqn. 16, the approximation to f(y) used by Grushka *et al.*[11], then eqn. 54 integrates to the simple analytical result

$$\lim_{\substack{B\to 0 \\ D_r(r)\to D_{ro}}} \frac{HD_{ro}\bar{v}}{(a\mu_o E)^2} = \frac{1}{1536}\left\{\frac{BB_A}{T_o}\right\}^2 \tag{55}$$

At first glance, eqn. 55 seems quite different from the result of Grushka *et al.*[11], which in dimensionless terms is

$$\lim_{\substack{B\to 0 \\ D_r(r)\to D_{ro}}} \frac{HD_{ro}}{a^2 u_m} = \frac{1}{24}\frac{(BB_A/T_o)^2}{(8 + BB_A/T_o)^2} \tag{56}$$

(This equation, as expressed in ref. 11, actually has a minus sign in the denominator, instead of a plus sign; this appears to be a typographical error.) The apparent difference between eqns. 55 and 56 arises from the neglect of electroosmotic flow in the derivation of eqn. 56, which makes the mean analyte velocity u_m different from the mean analyte velocity $\bar{v}$ described here. One can easily show

$$\lim_{\substack{B\to 0 \\ D_r(r)\to D_{ro}}} \frac{(\mu_o E)^2}{\bar{v}} = \frac{64\ u_m}{(8 + BB_A/T_o)^2} \tag{57}$$

when $\mu_{eo} = 0$ and $\bar{v}$ is calculated from eqns. 16 and 22. By substituting eqn. 57 into eqn. 55, one does obtain eqn. 56, as expected. One should perhaps observe that the inclusion of the electroosmotic flow is essential to an accurate description of plate height, even though it causes no dispersion. The flow does affect the analyte residence time and consequently the number of diffusive steps which partially average out differences in analyte velocity.

In conclusion of this section, one should note that the accuracy of the theory developed by Grushka *et al.*[11] should be substantially improved by substituting the right-hand side of eqn. 17 for B_A in eqns. 55 and 56. This substitution corrects these

authors' otherwise sound work for the shortcomings of the Andrade equation, with the result

$$\lim_{\substack{B\to 0\\ D_r(r)\to D_{ro}}} \frac{HD_{ro}\bar{v}}{(a\mu_o E)^2} = \frac{1}{1536}\left[(\ln 10)\beta_1 T_o B/(T_o - 168)^2\right]^2 \tag{58a}$$

$$\lim_{\substack{B\to 0\\ D_r(r)\to D_{ro}}} \frac{HD_{ro}}{a^2 u_m} = \frac{1}{24}\frac{\left[(\ln 10)\beta_1 T_o B/(T_o - 168)^2\right]^2}{\left[8 + (\ln 10)\beta_1 T_o B/(T_o - 168)^2\right]^2} \tag{58b}$$

where β_1 is defined by eqn. 12b. One notes that eqn. 58a is simply the first of the two terms comprising eqn. 53, which approximately corrects for the radial variation of the diffusion coefficient. The percentage error between eqns. 55 and 58a is

$$\lim_{\substack{B\to 0\\ D_r(r)\to D_{ro}}} \{[B_A(T_o - 168)^2/\ln(10)\beta_1 T_o^2]^2 - 1\}100 \tag{59}$$

and is a function of T_o only.

PROCEDURES

Numerical approximations to $\theta(y)$, eqn. 6a, were computed for specific values of B and T_o as detailed in Part I of the Theory section. Unless otherwise stated, f[T_o, $\theta(y)$] was calculated from eqn. 12. Numerical solutions to $\theta(y)$ were iteratively calculated, until $\theta(y)$ differed by less than one part in two thousand from its predecessor. For small B values (*e.g.*, $B = 0.0001$), only two or three iterations were required; for large B values (*e.g.*, $B = 0.40$), 20 to 25 iterations were required. The dimensionless non-equilibrium plate height, $HD_{ro}\bar{v}/(a\mu_o E)^2$, was then calculated from eqn. 50 with the numerical approximations to f(y) and $\theta(y)$ so determined. For purposes of comparison, $HD_{ro}\bar{v}/(a\mu_o E)^2$ was also computed from eqn. 54, in which the radial variation of the diffusion coefficient is ignored. Here, f(y) was also computed iteratively. This sequence of calculations was then repeated for other values of B and T_o. All numerical integrations were implemented with Simpson's rule and 399 discrete values of y, f(y), h(y), and $\theta(y)$. The computer program prerequisite to these computations was written in double-precision FORTRAN 77 and executed on the IBM 3081-GX computer at Southern Illinois University.

RESULTS AND DISCUSSION

Fig. 1 is a plot of log B *vs.* T_o for select values of radius a and 0.01 and 0.05 M phosphate buffers (pH 7.0), which are representative of those used by Jorgenson and Lukacs in their initial studies[28,29]. These B values were calculated from eqn. 4 with the

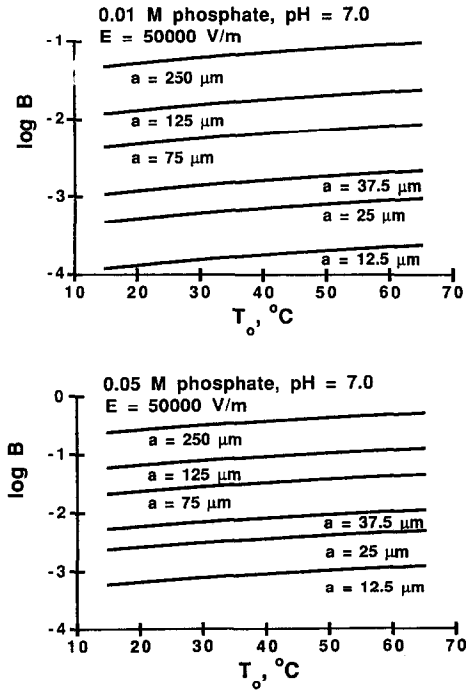

Fig. 1. Plots of log B *vs.* T_o for select capillary radii a, E = 50 000 V/m, and 0.01 and 0.05 M phosphate buffers (pH 7.0). Values of B were calculated from eqn. 4 as detailed in the text.

indicated a values, appropriate values of $k_{to}(T_o)$ and $k_{eo}(T_o)$, and E = 50 000 V/m. In these calculations, $k_{to}(T_o)$ was calculated from eqn. 7c, whereas $k_{eo}(T_o = 25°C)$ was calculated from eqn. 8, the electrophoretic mobilities of the $H_2PO_4^-$, HPO_4^{2-}, and PO_4^{3-} ions at infinite dilution[30], and the concentrations of these ions, which were determined from the acid dissociation constants of phosphoric acid at 25°C[31] and mass balance. The values of k_{eo} at other temperatures were then estimated by correcting k_{eo} (T_o = 25°C) for the variation of viscosity with temperature. Because the relationship between viscosity and temperature is almost exponential, the graphs of log B *vs.* T_o are almost linear. Although the field strength E one uses in these calculations is arbitrary, only a few studies have been carried out with E values greater than 50 000 V/m (ref. 32). Hence, almost all B values actually will be smaller than these, under otherwise identical conditions. These plots show that under typical experimental conditions (*e.g.*, buffer concentrations less than 0.05 M; radii less than 37.5 μm; field strengths less than 50 000 V/m), B is less than 0.01.

Fig. 2 is a plot of $\theta(y)/B$ *vs.* y for select values of B and T_o = 25°C. The lowermost bold curve is a graph of eqn. 5, which applies as B approaches zero. The other curves were computed with the iterative numerical algorithm described in Part I. To confirm this algorithm, the numerical solutions to $\theta(y)$ so computed were compared to the Bessel functions proposed by Coxon and Binder[16], Brown and Hinckley[17], and Jones and Grushka[18]. No substantial difference exists between these solutions, as long as $B < 0.20$; for larger B values, the variation of f(y) with $\theta(y)$ is no longer linear and Bessel functions no longer apply. (These comparisons were actually made by setting

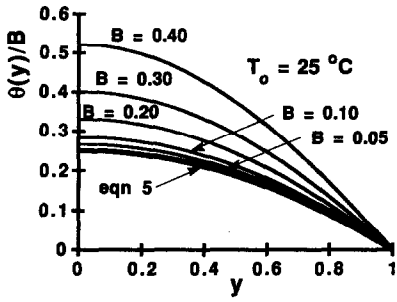

Fig. 2. Plot of $\theta(y)/B$ *vs.* y for select values of B and $T_o = 25°C$. The lowermost bold curve was calculated from eqn. 5; the other curves were computed numerically.

$h[T_o,\theta(y)]$ to unity, since Bessel functions apply when the thermal conductivity is constant. If one allows $h[T_o,\theta(y)]$ to vary with temperature, the Bessel functions are actually acceptable solutions up to $B = 0.30$ or so, because this variation partially compensates for error.) It is unlikely that a flawed algorithm would make predictions that so closely agree with theory. In general, the algorithm always appears to converge to the appropriate global solution to $\theta(y)$; no erroneous local solutions were ever computed in these comparisons.

One can conclude from Fig. 2 that eqn. 5 is a fairly good approximation to $\theta(y)$ for values of B less than 0.01 or so. For much larger B values, however, this solution is clearly inadequate. By comparing the numerical solutions to $\theta(y)/B$ for various B values, one infers that their departure from eqn. 5 is non-linear in B (*e.g.*, the difference between the values of $\theta(y)/B$ at $y = 0$ for $B = 0.40$ and $B = 0.20$ is more than twice the corresponding difference for $B = 0.20$ and eqn. 5, which applies as $B \to 0$). The principal relevance of these departures to this work is the inadequacy of the analytical approximations to $f(y)$, eqns. 13 and 16, when B is greater than 0.01 or so. These approximations are inadequate because they were derived with eqn. 5, which is invalid under these circumstances.

Fig. 3 is a plot of $[f(y)-1]/B$ *vs.* y for select values of B and $T_o = 25°C$. The lowermost bold curve in the upper figure (Fig. 3a) was calculated from eqn. 13, the analytical approximation to $f(y)$ derived here. The dashed bold curve in this figure, and the lowermost bold curve in the lower figure (Fig. 3b), were calculated from eqn. 16 ($B_A = 2400$ K), the analytical approximation to $f(y)$ derived from the Andrade equation. Clearly, these approximations differ at this T_o, and this difference increases with increasing T_o (see below). Because this figure effectively represents the variation of electrophoretic mobility (less the mobility at the wall) with the radial coordinate, one concludes that substantial differences will exist between plate heights calculated from these two functions, even for vanishingly small values of B.

The remaining curves in Fig. 3a and b were computed numerically. In Fig. 3a, $f[T_o,\theta(y)]$ was calculated from eqn. 12, whereas in Fig. 3b, $f[T_o,\theta(y)]$ was calculated from eqn. 15. The numerical solutions to $f(y)$ do not substantially differ from the appropriate analytical one, as long as B is less than 0.01 or so. This finding is perhaps not surprising, because the function $\theta(y)$, on which $f[T_o,\theta(y)]$ depends, can be approximated under these conditions by eqn. 5. For larger values of B, however, the numerical solutions to $f(y)$ differ substantially from the analytical ones. As with $\theta(y)$,

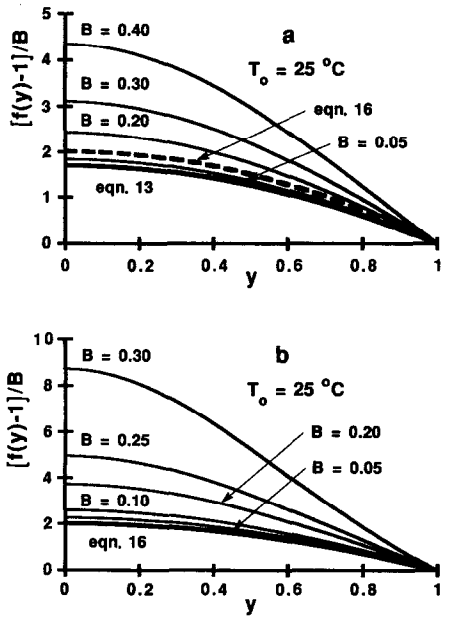

Fig. 3. Plots of $[f(y)-1]/B$ *vs.* y for select values of B and $T_o = 25°C$. The lowermost bold curve in (a) was calculated from eqn. 13; the dashed bold curve in (a), and the lowermost bold curve in (b), were calculated from eqn. 16. The other curves were computed numerically, with $f[T_o,\theta(y)]$ expressed by eqn. 12 for the curves in (a) and by eqn. 15 for those in (b).

the departures of the numerical solutions to $f(y)$ from the analytical ones are non-linear in B. More importantly, significant deviations between Fig. 3a and b are found as B increases. For example, when $B = 0.30$, the value of $[f(y)-1]/B$ at $y = 0$ in Fig. 3a is 3.10, whereas the corresponding value in Fig. 3b is 8.73. These large deviations indicate the necessity of describing η correctly for large B values. The principal origin of these deviations is the overestimation of $f[T_o,\theta(y)]$ by eqn. 15, which in turn causes the functions $\theta(y)$ and $f(y)$ to be overestimated. By the time these functions have converged, after many iterations of the numerical algorithm, these overestimations have been amplified many times.

As another test of the algorithm developed here, a numerical solution to $f(y)$ for $B = 0.0001$ was iteratively computed and compared to the analytical solution, eqn. 13. One would expect little difference between these solutions, since $B \ll 0.01$. In fact, these solutions differed beyond only the seventh or eighth significant figure. In other words, an extremely accurate solution to $f(y)$ was calculated numerically. The author believes that this test confirms this algorithm beyond any reasonable doubt.

Fig. 4 is a plot of the logarithm of the dimensionless plate height, $\log HD_{ro}\bar{v}/(a\mu_o E)^2$, *vs.* $\log B$ for select values of T_o. The abscissa, $\log B$, in each graph is limited by the boiling point of the buffer; therefore, $\log B$ is largest for the smallest T_o values. Because the curves only slightly differ for different T_o values, they are graphed either on different axes or in different plots. The solid curves are graphs of eqn. 50, which corrects for the radial variation of the diffusion coefficient; the dashed curves are graphs of eqn. 54, in which this variation is ignored. For B values less than 0.01 or

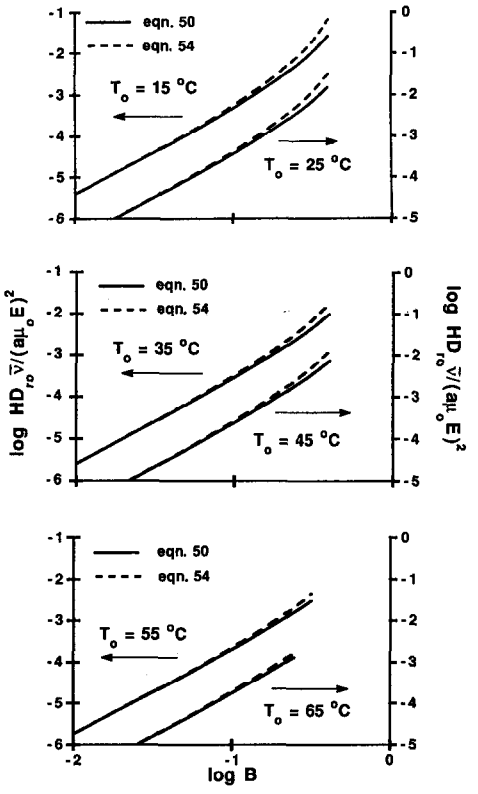

Fig. 4. Plots of log $HD_{ro}\bar{v}/(a\mu_o E)^2$ *vs.* log B for select values of T_o. Solid curves were computed from eqn. 50; dashed curves were computed from eqn. 54. The former equation corrects for the radial variation of the diffusion coefficient; the latter does not.

so, $HD_{ro}\bar{v}/(a\mu_o E)^2$ varies linearly with B^2 (*i.e.*, the slope of the log $HD_{ro}\bar{v}/(a\mu_o E)^2$ *vs.* log B plot is two), although this variation is not shown to avoid the loss of other details. Furthermore, the radial variation of the diffusion coefficient has no significant effect on the plate height. For B values greater than 0.01 or so, however, $HD_{ro}\bar{v}/(a\mu_o E)^2$ varies more rapidly with B than B^2, because $\theta(y)$ and $f(y)$ vary with a power of B greater than one (see above). More importantly, for B values greater than 0.01 or so, the radial variation of the diffusion coefficient also affects the plate height, and this effect increases with increasing B. In these cases, the temperature near the capillary center rises sufficiently above T_o to substantially increase diffusion in this region, relative to that near the wall. Because the time required for analyte ions to diffuse between various positions in the capillary is correspondingly reduced, the differences in analyte velocity at these positions are more effectively averaged out and the plate height decreases.

Because the radial variation of the diffusion coefficient does not significantly affect $HD_{ro}\bar{v}/(a\mu_o E)^2$ unless B is greater than 0.01 or so, one concludes that eqns. 51 and 53, which analytically correct for this variation, have little use. This lack of utility exists, because the analytical approximations to $f(y)$ and $\theta(y)$ with which these equations were derived are themselves not valid, when B is greater than 0.01 or so.

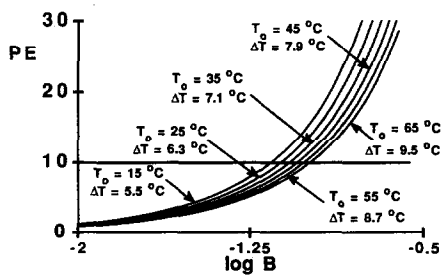

Fig. 5. Plot of percentage error PE between eqns. 50 and 54 *vs.* log B for select values of T_o. The former equation corrects for the radial variation of the diffusion coefficient; the latter does not.

A comparison of the values of $HD_{ro}\bar{v}/(a\mu_o E)^2$ computed numerically from eqn. 50 to those calculated from eqn. 53 confirms this finding. (Much numerical error is encountered in the evaluation of eqn. 51 for small B values, even in double-precision FORTRAN; hence, these results are not compared to eqn. 50.) Unfortunately, with the theory developed here, one cannot determine a simple analytical correction to plate height theory which holds when the radial variation of the diffusion coefficient is important.

The differences between the corrected and uncorrected values of $HD_{ro}\bar{v}/(a\mu_o E)^2$ in Fig. 4 are perhaps underemphasized because of the logarithmic scale. Fig. 5 is a plot of the percentage error, PE, between eqns. 50 and 54 *vs.* log B for select values of T_o. The radial variation of the diffusion coefficient is accounted for in the former equation, whereas this variation is "turned off" in the latter equation. To evaluate both equations, the functions $f(y)$ and $\theta(y)$ were computed numerically, because B is greater than 0.01. The percentage error between these equations is less than one or so, when B is less than 0.01, but rapidly increases with increasing B. The rapid rate of this increase is not apparent from the figure, which is compressed in the vertical direction to avoid loss of detail. For example, the value of PE for $T_o = 15°C$ and $\log B = -0.40$ ($B = 0.40$) slightly exceeds 150.

An arbitrary percentage error, above which one might wish to correct for the variation of the diffusion coefficient, is indicated in Fig. 5 by the horizontal line at PE = 10. The calculated temperature differences ΔT between the capillary center and wall at this threshold are indicated in the figure for the various T_o values. These differences, which are greater than 5°C, are nearly a linear function of T_o (the increment is 0.8°C per 10°C increase in T_o). By and large, this threshold is not crossed, unless B is greater than 0.08 ($\log B > -1.1$) or so. Because experimental values of B almost invariably will be less than this value (see Fig. 1), one can typically neglect the variation of the diffusion coefficient and use the simpler equations for plate height referenced in the Introduction, in which this variation is ignored. Thus, in one sense, the extensive theory derived above may seem somewhat academic. Yet, one must bear in mind that the numerical rigor supporting the conclusion just drawn would not have been possible without it.

Fig. 6 is a plot of $HD_{ro}\bar{v}/(a\mu_o E)^2$ *vs.* log B for select values of T_o. Unlike in Fig. 4, the curves here are not corrected for the variation of the diffusion coefficient. The solid curves, the curves comprised of short dashes, and the curves comprised of long dashes

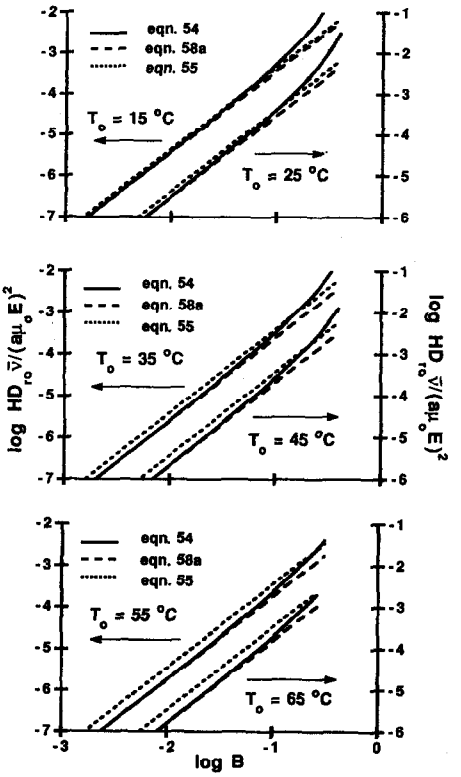

Fig. 6. Plots of log $HD_{ro}\bar{v}/(a\mu_o E)^2$ *vs.* log B for select values of T_o. The solid curves, the curves comprised of short dashes, and the curves comprised of long dashes are graphs of eqns. 54, 55 (B_A = 2400 K) and 58a, respectively. None of these curves corrects for the radial variation of the diffusion coefficient.

are graphs of eqns. 54, 55 (B_A = 2400 K) and 58a, respectively. The last two equations are analytical approximations to the first, which was evaluated numerically. Eqn. 58a, in which f(y) is expressed by eqn. 13, agrees well with this numerical solution, when B is

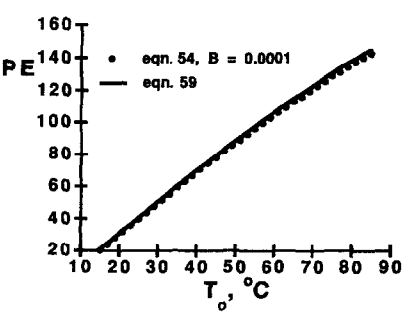

Fig. 7. Plot of percentage error PE between the solutions of Grushka *et al.*[11] and those developed here *vs.* T_o for small B values. Circles represent computations from eqn. 54 and B = 0.0001; the curve is a graph of eqn. 59 (B_A = 2400 K).

less than 0.01 or so, but differs with increasing B. Furthermore, the predictions of eqns. 55 and 58a significantly differ, even when $B \ll 0.01$. (Eqn. 55, in which $f(y)$ is expressed by eqn. 16, is equivalent to the result derived by Grushka *et al.*[11], except that electroosmotic flow is included.) This difference increases with increasing T_o and originates solely from the choice of the function $f(y)$ with which one evaluates eqn. 54. Because eqn. 16 is greater than eqn. 13 (see Fig. 3a), the values of $HD_{ro}\bar{v}/(a\mu_o E)^2$ predicted by eqn. 55 are greater than those predicted by eqn. 58a.

The differences between the values of $HD_{ro}\bar{v}/(a\mu_o E)^2$ derived here and predicted by Grushka *et al.*[11] are perhaps underemphasized in Fig. 6, because of the logarithmic scale. Fig. 7 is a plot of the percentage error PE between these values *vs.* T_o for $B \ll 0.01$. The circles represent the percentage error computed numerically from eqn. 54, when $B = 0.0001$ and $f[T_o,\theta(y)]$ was alternatively represented by eqns. 12 and 15. The solid curve is a graph of eqn. 59 ($B_A = 2400$ K), which clearly approximates this error. This error substantially increases with increasing T_o and is greater than 100% for $T_o > 50$°C or so, a value that is not that uncommon experimentally[33,34].

CONCLUSIONS

The principal significance of this work is its validation of previous analytical solutions to the non-equilibrium plate height in capillary zone electrophoresis. The fairly rigorous treatment developed here, which is based on an iterative solution to the steady-state equation of heat conduction and the inclusion in the continuity equation of the radial variation of diffusion coefficient, does not differ from simpler analytical ones, unless the temperature difference between the capillary center and wall substantially exceeds that encountered in practice. This work also establishes the range of the parameter B over which these analytical solutions apply and suggests that the Andrade equation can mislead one about values of electrophoretic mobility and non-equilibrium plate height, especially at elevated temperatures.

A shortcoming of this work is the lack of any relationship between the temperature T_o of the capillary wall and the ambient temperature of the capillary surroundings. The latter is easily measured, whereas the former is not. Therefore, some relationship between the two is prerequisite to the testing of this theory. Others have addressed this problem[11,16–18] and their results can be easily adapted here.

No theory is better than the assumptions on which it rests. Most of the assumptions made here (*e.g.*, the absence of thermal diffusion, the absence of heat transfer from electroosmotically induced forced convection, and the independence of chemical equilibria of temperature) are fairly reasonable ones. The assumption of a vanishingly small analyte concentration may be subject to criticism, since in practice one works with detectable levels of analyte, which can affect plate numbers[29]. For better or worse, others have made this assumption and the author has made it as well. Perhaps in this light, this study should be viewed as more comparative than definitive.

One may wish to investigate more closely the assumption of negligible thermal (*i.e.*, free) convection, because the ΔT values reported in Fig. 5 are somewhat substantial. Experiments in wide-bore capillaries have clearly demonstrated the necessity of rotating the capillary contents to minimize dispersion by free convection[7]. A detailed evaluation of the expected amount of free convection is beyond the author's

ability. A rough evaluation is gained by calculating the dimensionless free-convective Nusselt number[14]

$$Nu \approx 0.5(PrGr)^{1/4} \tag{60}$$

where $Pr = C_p\eta/k_t$ and $Gr = a^3g\delta\Delta T/\lambda^2$ are the dimensionless Prandtl and Grashof numbers. (In these definitions, the parameters g, C_p, δ, and λ are the acceleration due to gravity and the constant-pressure heat capacity, thermal coefficient of expansion, and kinematic viscosity of the buffer.) At 25°C, the Prandtl number of dilute aqueous buffers is about 6.16 [$C_p = 4180$ J/kg K, $\eta = 8.90 \cdot 10^{-4}$ kg/ms, and $k_t = 0.605$ W/m K (ref. 35)], whereas the Grashof number can be approximated as $3.16 \cdot 10^9 \Delta T a^3$ [$g = 9.81$ m/s^2, $\delta = 2.57 \cdot 10^{-4}$ K^{-1}, and $\lambda = 8.93 \cdot 10^{-7}$ m^2/s (ref. 35)]. Fig. 5 indicates that ΔT will rarely exceed 10°C = 10 K, whereas a will rarely, if ever, exceed $2.5 \cdot 10^{-4}$ m. Thus, Nu is expected to be less than 0.65 or so. According to the author of ref. 36, this value of Nu indicates that free convection should be minor.

In spite of the rigor of these calculations, they remain at best approximate, because the viscosities of the buffers used in capillary zone electrophoresis are greater than the viscosity of pure water. Furthermore, the variations with temperature of the viscosities of pure water and buffers most probably differ. In these calculations, one has implicitly assumed they are equal. In general, the error so introduced depends on the buffer type and concentration and consequently is difficult to quantify. One can, however, gauge the magnitude of this error by a simple calculation. The viscosity of a 0.051 M solution of phosphoric acid at 20°C is about 1.010 cp (ref. 35), which is 0.008 cp greater than the viscosity of water at this temperature (1.002 cp). If one modifies the numerical algorithm to increment η by 0.008 cp during each iteration, such that $f[T_o, \theta(y)]$ is appropriately adjusted, one finds that the values of $HD_{ro}\bar{v}/(a\mu_o E)^2$ so computed differ from previous computations by less than 4%, when 15°C $< T_o <$ 65°C and $B < 0.01$. Clearly, this calculation is greatly oversimplified. It does suggest, however, that the increased viscosity has only a small effect, as long as the buffer concentration is less than 0.05 M.

SYMBOLS

A_i	f_{ri}/η (m)
A_i^*	$z_i^2 C_i$ (mol/m^3)
A'	$D_r(r)\eta(r)/T(r)$ (kg m/s^2 K)
a	capillary radius (m)
B	$k_{eo}a^2E^2/k_{to}T_o$
B_A	empirical temperature in Andrade equation, commonly equated to 2400 K
c	analyte concentration (mol/m^3)
$c_m(z_1)$	cross sectional average concentration (mol/m^3)
C_i	concentration of ith buffer ion (mol/m^3)
C_p	constant-pressure heat capacity (J/kg K)
$D_r(r)$	radial diffusion coefficient (m^2/s)
D_{ro}	radial diffusion coefficient at inner capillary wall (m^2/s)

D_z	axial diffusion coefficient (m^2/s)
$\mathscr{D}$	effective diffusion coefficient (m^2/s)
e	fundamental electrical charge (C)
E	electric field strength (V/m)
$f(y)$; $f(r)$	$k_e(y)/k_{eo}$; $k_e(r)/k_{eo}$
$f[T_o,\theta(y)]$	$k_e[T_o,\theta(y)]/k_{eo} = \eta_o/\eta[T_o,\theta(y)]$
f_r; f_{ri}	friction coefficient; friction coefficient of ith ion (kg/s)
F	Faraday (C/mol)
g	acceleration due to gravity (m/s^2)
$g(y)$; $g(r)$	function defined by eqns. 36 and 37 (m)
$g(0)$	value of $g(y)$ and $g(r)$ at $y = r = 0$ (m)
$h(y)$	$k_t(y)/k_{to}$
$h[T_o,\theta(y)]$	$k_t[T_o,\theta(y)]/k_{to}$
H	non-equilibrium plate height (m)
$HD_{ro}\bar{v}/(a\mu_o E)^2$	dimensionless non-equilibrium plate height
$k_e(r)$; $k_e(y)$	electrical conductivity (mho/m)
k_{eo}	electrical conductivity at inner capillary wall (mho/m)
$k_t(r)$; $k_t(y)$	thermal conductivity (W/m K)
k_{to}	thermal conductivity at inner capillary wall (W/m K)
N_r	radial flux (mol/m^2 s)
N_z	axial flux (mol/m^2 s)
r	radial coordinate (m)
t	time (s)
T	temperature (K or °C)
T_o	temperature at inner capillary wall (K or °C)
u_m	average elctrophoretic mobility in theory of Grushka *et al.*[11] (m^2/V s)
$\bar{v}$	average zone velocity (m/s)
v_r	radial velocity (m/s)
$v_z(r)$; $v_z(y)$	axial velocity (m/s)
y	r/a
z	axial coordinate (m)
z_i	unsigned charge number of ith ion
z_1	$z - \bar{v}t$ (m)
α	$\ln(10)\beta_1 T_o/(T_o - 168)^2$
α_1, α_2	coefficients of $h(T_o,\theta)$ defined by eqn. 7a and b
β_1, β_2, β_3	coefficients of $h(T_o,\theta)$ defined by eqn. 12b–d
δ	coefficient of thermal expansion of buffer (K^{-1})
Δ	thermal conductivity of water (W/m K)
ΔT	temperature difference between capillary center and wall (°C)
ε	electrical permittivity (F/m)
ζ	zeta potential (V)
η	viscosity (kg/m s)
η_o	viscosity at inner capillary wall (kg/m s)
η^*	$\eta e^{-B_A/T}$ (kg/m s)
$\theta(y)$; $\theta(r)$	$[T(y)-T_o]/T_o$; $[T(r)-T_o]/T_o$
λ	kinematic viscosity (m^2/s)

μ	electrophoretic mobility (m^2/V s)
μ_{eo}	electroosmotic flow coefficient (m^2/V s)
μ_o	electrophoretic mobility at inner capillary wall (m^2/V s)

ACKNOWLEDGEMENT

The author gratefully acknowledges Dr. David W. Kammler of the Department of Mathematics at Southern Illinois University for his suggestion of an iterative numerical solution to eqn. 6a.

REFERENCES

1 B. P. Konstantinov and O. V. Oshurkova, *Sov. Phys.-Techn. Phys.*, 11 (1966) 693.
2 G. Taylor, *Proc. Roy. Soc. (London)*, 219A (1953) 186.
3 G. Taylor, *Proc. Roy. Soc. (London)*, 225A (1954) 473.
4 A. J. P. Martin and F. M. Everaerts, *Proc. Roy. Soc. (London)*, 316A (1970) 493.
5 M. J. E. Golay, in D. H. Desty (Editor), *Gas Chromatography, 1958*, Academic Press, New York, NY, 1958.
6 H. C. Cox, J. K. C. Hessels and J. M. G. Teven, *J. Chromatogr.*, 66 (1972) 19.
7 S. Hjertén, *Chromatogr. Rev.*, 9 (1967) 122.
8 R. Aris, *Proc. Roy. Soc. (London)*, 235A (1956) 67.
9 R. Virtanen, *Acta Polytech. Scand.*, 123 (1974) 7.
10 J. H. Knox and I. H. Grant, *Chromatographia*, 24 (1987) 135.
11 E. Grushka, R. M. McCormick and J. J. Kirkland, *Anal. Chem.*, 61 (1989) 241.
12 N. S. Reejhsinghani, A. J. Barduhn and W. N. Gill, *J. AIChE*, 14 (1968) 100.
13 J. C. Giddings, *Dynamics of Chromatography*, Marcel Dekker, New York, NY, 1965.
14 R. B. Bird, W. E. Stewart and E. N. Lightfoot, *Transport Phenomena*, Wiley, New York, NY, 1960, p. 272.
15 H. S. Carslaw and J. C. Jaeger, *Conduction of Heat in Solids*, Clarendon, Oxford, 2nd ed., 1986.
16 M. Coxon and M. J. Binder, *J. Chromatogr.*, 101 (1974) 1.
17 J. F. Brown and J. O. N. Hinckley, *J. Chromatogr.*, 109 (1975) 218.
18 A. E. Jones and E. Grushka, *J. Chromatogr.*, 466 (1989) 219.
19 R. W. Powell, C. Y. Ho and P. E. Liley, in R. C. Weast (Editor), *CRC Handbook of Chemistry and Physics*, CRC Press, Boca Raton, FL, 69th ed., 1988, p. E-11.
20 R. C. Reid, J. M. Prausnitz and B. E. Poling, *The Properties of Gases and Liquids*, McGraw-Hill, New York, 4th ed., 1987.
21 A. J. Bard and L. R. Faulkner, *Electrochemical Methods*, Wiley, New York, NY, 1980.
22 J. F. Swindells, in R. C. Weast (Editor), *CRC Handbook of Chemistry and Physics*, CRC Press, Boca Raton, FL, 69th ed., 1988, p. F-40.
23 J. R. Coe Swindells, Jr. and T. B. Godfrey, *J. Res.*, 48 (1952) 1.
24 R. J. Hunter, *Zeta Potential in Colloid Science: Principles and Applications*, Academic Press, London, 1981.
25 T. K. Sherwood, R. L. Pigford and C. R. Wilke, *Mass Transfer*, McGraw-Hill, New York, NY, 1975.
26 J. C. Giddings, *J. Chem. Phys.*, 49 (1968) 81.
27 J. C. Giddings, Y. H. Yoon, K. D. Caldwell, M. N. Myers and M. E. Hovingh, *Sep. Sci.*, 10 (1975) 447.
28 J. W. Jorgenson and K. D. Lukacs, *Anal. Chem.*, 53 (1981) 1298.
29 K. D. Lukacs and J. W. Jorgenson, *J. High Resolut. Chromatogr. Chromatogr. Commun.*, 8 (1985) 407.
30 C. M. Mason and J. B. Culvern, *J. Am. Chem. Soc.*, 71 (1949) 2387.
31 D. A. Skoog, D. M. West and F. J. Holler, *Fundamentals of Analytical Chemistry*, Saunders College Publishing, New York, 5th ed., 1988.
32 F. Foret, M. Deml and P. Becek, *J. Chromatogr.*, 452 (1988) 601.

33 S. Terabe, K. Otsuka and T. Ando, *Anal. Chem.*, 57 (1985) 834.
34 J. W. Jorgenson, in J. W. Jorgenson and M. Phillips (Editors), *New Directions in Electrophoretic Methods, (ACS Symposium Series*, No. 335), American Chemical Society, Washington, DC, 1987.
35 R. C. Weast (Editor), *CRC Handbook of Chemistry and Physics*, CRC Press, Boca Raton, FL, 69th ed., 1988.
36 H. A. Pohl, *Dielectrophoresis*, Cambridge University Press, Cambridge, 1978.